Applied Materials Today 19 (2020) 100542

Contents lists available at ScienceDirect

Applied Materials Today

journal homepage: www.elsevier.com/locate/apmt

Ultrafast self-healing and highly transparent coating with mechanically durable icephobicity

Yizhi Zhuo, Senbo Xiao*, Verner Håkonsen, Tong Li, Feng Wang, Jianying He*, Zhiliang Zhang*

NTNU Nanomechanical Lab, Department of Structural Engineering, Norwegian University of Science and Technology (NTNU), Trondheim, 7491, Norway

ARTICLE INFO

Article history:
Received 19 September 2019
Received in revised form 9 December 2019
Accepted 19 December 2019

Keywords:
Icephobicity
Self-healing
Transparency
Recyclability
Anti-icing

ABSTRACT

Excessive ice accretion on infrastructures can lead to severe damage and dysfunction. In the context of combating the build-up of unwanted icing and at the same time maintaining sunlight transmission, for instance on solar panels, windows and sensors, mechanically durable and transparent icephobic coatings are highly desired. Herein, we design and fabricate an icephobic coating possessing for the first time combined properties of ultrafast self-healing and outperforming transparency. Our coating can restore more than 80 % of the ultimate tensile strength within 45 min of healing at room temperature after introducing a cut. By a combination of both experiments and atomistic simulations, we establish the atomistic mechanism for ultrafast self-healing, *i.e.* the optimal balance between polymer chain flexibility and concentration of hydrogen bonding pairs. Equipped with such ultrafast self-healing property, the coating shows a stable ice adhesion strength of 52.2 ± 8.9 kPa after 20 icing/deicing cycles, and 48.2 ± 4.6 kPa after healing from mechanical damage, exhibiting exceptional robustness for anti-icing applications that require high mechanical endurance. Importantly, the coating on glass shows a light transmittance of 89.1 % in the visible region, which is remarkably close to bare glass (91.9 %). Moreover, the coating is recyclable due to the dissociable crosslinks, providing a sustainable aspect missing in existing state-of-the-art icephobic coatings. This coating combines the properties of icephobicity, mechanical durability (*via* self-healing), transparency and recyclability, and thus enlightens the design of multifunctional materials for meeting complex environmental requirements encountered in the field of anti-icing.

1. Introduction

Excessive accumulation of ice and snow has a severe effect on infrastructures and transportation, including airplanes, marine structures, wind turbines, power lines and many others [1–8]. Specifically, the build-up of unwanted icing on the exposed surfaces can block the passage of light to the surfaces, leading to the dysfunction of apparatus that require high light transmission, such as solar panels, windows and sensors [9]. Traditional methods for ice removal, for instance by active heating or using anti-freezing fluids are known to be energy-intensive and could yield unsolvable environmental problems [10]. Recently, various surfaces with low ice adhesion strength (<100 kPa) were developed to mitigate the icing problem [2,11–15]. However, to continuously protect the surfaces that desire optical transparency, low ice adhesion strength is not enough. Mechanical durability and high transparency should be also integrated into the coating. Nevertheless, the mechanical durability of these icephobic surfaces remains an unresolved issue, especially in the outdoor applications where these surfaces are exposed to abrasion and scratches. Mechanical damage can easily develop in these new surfaces in the de-icing process, which further induce strong ice adhesion caused by ice-surface interlocking, significantly shortening the lifespan of the anti-icing functionality [16]. Introducing self-healing function into icephobic surfaces is an effective strategy to address the interlocking effect induced by mechanical damage, which is also a practical approach for durability of surface icephobicity [16,17]. Currently, self-healing icephobic coatings require high temperature or a long self-healing time to restore mechanical damage [16,17]. It is thus important to understand the determinants of self-healing and to seek rational design principles to optimize self-healing materials for the purpose of anti-icing. Furthermore, coating transparency, which is highly desired in specific application areas is still a missing property in the previously reported self-healing icephobic materials [9,16,17]. Hence, developing an icephobic surface with combined outperforming self-healing rate and high optical transparency is in urgent need.

* Corresponding authors.
E-mail addresses: senbo.xiao@ntnu.no (S. Xiao), jianying.he@ntnu.no (J. He), zhiliang.zhang@ntnu.no (Z. Zhang).

https://doi.org/10.1016/j.apmt.2019.100542
2352-9407/

There are many methods to realize self-healing, for example high temperature oxidation [18], the addition of a self-healing agent [19] and incorporating polymer with dynamic bonds [20–28]. High temperature oxidation requires ultrahigh temperature (such as 1200 °C) to form metallic oxide to fill the damage [18]. The materials that based on adding self-healing agents and incorporating polymer with dynamic bonds can also be named as extrinsic and intrinsic healing materials, respectively [27,29,30]. The extrinsic healing polymers contain pre-embedded encapsulated reactive agents which release at the cracking interfaces to fill and repair the damage [19,28,31]. The self-healing property of these extrinsic healing polymers is efficient, but usually has a limited number of healing cycles owing to the exhaustion of the reactive agents [32]. In contrast, the intrinsic healing polymers repair mechanical damage by formation of dynamic bonds, such as hydrogen bonds [20–23], metal-ligand coordination [24], ionic interactions [25], disulfide bridges [26,27], and key-and-lock van der Waals forces [28]. The intrinsic healing materials thus possess a non-exhaustible self-healing property, which is more suitable for materials under requirements of long operation lifespans, such as icephobic materials. The self-healing process of the intrinsic healing polymers is a diffusion-reaction process of polymer chains, which contains three stages [33], namely the generation of reactive sites, followed by the diffusion of polymer chains, and finally the reformation of dynamic bonds (reaction) [34]. Previous reports have found that polymers with non-crystalline structures displayed higher self-healing rates than those with tightly packed crystalline molecular structures, which reveals the effect of crystal structure on restricting chain segmental motion (diffusion) accounting for low self-healing efficiency [27,29]. These results have demonstrated the significance of the flexibility of chains. Driven by positive entropy change and network density gradients near damaged areas, the polymer chains will continuously diffuse into each other, thus filling the damage [34]. During this process, dynamic bonds will form when the reactive sites are encountered, to strengthen the damaged interface. However, in turn, the formed dynamic bonds will hamper the further diffusion of polymer chains. Hence, not only can the flexibility of polymer chains affect the healing of damage, but also the concentration of reactive sites. This means that flexible polymer chain with optimal concentration of reactive sites should be designed to realize fast self-healing.

Herein, by adopting flexible and colourless polymer segments as well as tuning the concentration of hydrogen bonding sites (c_H), we designed and fabricated an icephobic coating with ultrafast self-healing rate and high transparency. Specifically, we first rationalized the two critical factors, chain diffusion and bonding site density, in the nanoscale mechanics of the self-healing interface by atomistic modelling and simulations. We then prepared a polydimethylsiloxane-urea (PDU) coating consisting of polydimethylsiloxane (PDMS) chains and urea groups (Fig. 1), serving as flexible segments and bonding sites, respectively. The PDMS chains contain asymmetric alicyclic segments by design, which are in favor of chain motion (diffusion) and thus fast self-healing. In addition, we tuned the molecular weight of the PDMS segment to control the concentration of hydrogen bonding sites, which is another key determinant of the self-healing property. Higher concentration of hydrogen bonding sites can lead to higher possibility of reformation of hydrogen bonds during self-healing, but can also render the increase of friction between polymer chains thus lower diffusion rate. We chose the urea groups to serve as dynamic crosslinkers (hydrogen bonds) in the coating not only for healing any possible mechanically damaged area in the coating, but also for their colorlessness to ensure high optical transparency.

Following our polymer design principle, the prepared coating exhibited ultrafast self-healing rate, recovering more than 80 % of the ultimate tensile strength within 45 min of healing upon cutting at room temperature. The ultrafast self-healing properties of the designed elastomer outperforms the results of other similar self-healing materials from previous studies [21,23,24,26,27,35,36]. Moreover, the self-healing coating on glass demonstrated high optical transparency, showing a transmittance of 89.1 % in the visible region which is close to bare glass (91.9 %). Owing to the hydrophobicity and the low Young's modulus of the polymer, the coating showed a low ice adhesion strength of 38.3 ± 0.5 kPa. Importantly, the coating icephobicity was found to be highly durable due to efficient self-healing, showing a stable low ice adhesion strength of 52.2 ± 8.9 kPa during 20 icing/de-icing cycles, and 48.2 ± 4.6 kPa after healing from purposely introduced mechanical damage. The sufficiently low ice adhesion, combined with the enhanced mechanical robustness, high light transparency as well as recyclability, make the coating suitable for practical applications in the field of anti-icing.

2. Results and discussion

2.1. Preparation of PDU

PDU was synthesized from commercially available isophorone diisocyanate (IDI) and bis(3-aminopropyl)-terminated PDMS (H_2N-PDMS-NH_2). In order to elucidate the effect of the length of free segments in polymer diffusion, three molecular weights of the PDMS segment, *i.e.* 1000, 3000, and 5000 Da, were chosen in the fabrication the PDU samples, as shown in Figs. 1 and S1. The resulting polymers were denoted as PDU1000, PDU3000, and PDU5000, respectively. To compare with a sample displaying the crystallization effect (which is non-existent in the PDU sample), H_2N-PDMS-NH_2 (molecular weight: 3000) with symmetric 4,4′-Methylenebis(phenyl isocyanate) (MPI), termed PDUM3000, was also fabricated (Fig. S1). The symmetric MPI units in the PDUM3000 is a strong promoter for crystallization in the as-prepared PDUM3000 sample. More details on the experiments are given in the Materials and Methods Section in Supplementary Materials. ^{1}H nuclear magnetic resonance (NMR) spectroscopy and attenuated total reflectance-Fourier transform infrared (ATR-FTIR) spectroscopy confirmed the successful synthesis of the polymers (Figs. S2 and S3). In addition, thermogravimetric analysis (TGA) demonstrated the thermal stability of PDU and PDUM, with no decomposition detected below 250 °C (Fig. S4).

As it is known that the intrinsic self-healing of polymers relies on the exchange of dynamic groups [22], the hydrogen-bonding interactions are highly relevant to the self-healing property of both the PDU and PDUM samples. The hydrogen-bonding interactions of the polymers were characterized by ATR-FTIR analysis in the temperature range of 30 °C–150 °C [22,37,38]. As depicted by the ATR-FTIR spectra shown in Figs. 2 and S5, the bands from ~1750 cm^{-1} to ~1600 cm^{-1} are ascribed to the amide I mode of the urea group of PDU and PDUM, while the bands from ~1575 cm^{-1} to ~1500 cm^{-1} are attributed to the amide II mode of the urea group [38]. In the amide I region of PDU (Fig. 2a–c), the peaks at 1628 cm^{-1}, attributed to the stretching of hydrogen bonded C=O, exhibit a blue-shift to 1636 cm^{-1} and reduction of intensity as temperature increases from 30 °C to 150 °C, while several peaks arise at higher wavenumber (1647, 1653 cm^{-1} and so on) synchronously. Such evolution of signals indicates the dynamic dissociation of hydrogen bonds. Furthermore, in the amide II region, with the rising temperature from 30 °C to 150 °C, the peaks of PDU (Fig. 2a–c) at 1572 cm^{-1} related to the in-plane bending of hydrogen bonded N–H decline, while several new peaks (at 1559, 1541 cm^{-1} and so on) increase. The corresponding signals monitored in the PDUM3000 sample are similar to the PDU samples (Fig. 2d). In addition, in the N–H

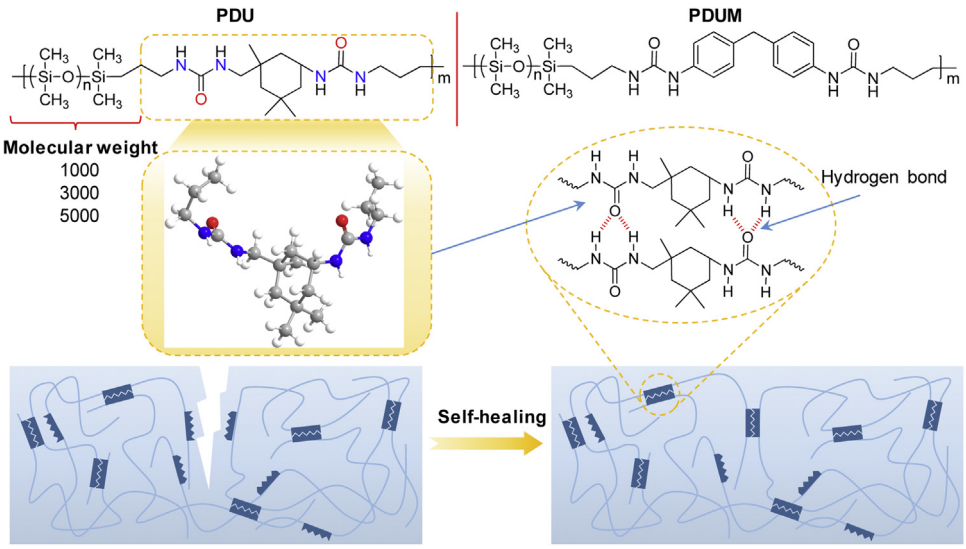

Fig. 1. Molecular structures and self-healing mechanism of PDU and PDUM. The different molecular weights of the PDMS segment for PDU are 1000, 3000 or 5000 Da, and 3000 Da for PDUM. Reformation of hydrogen bonds at the cut interface facilitates the self-healing.

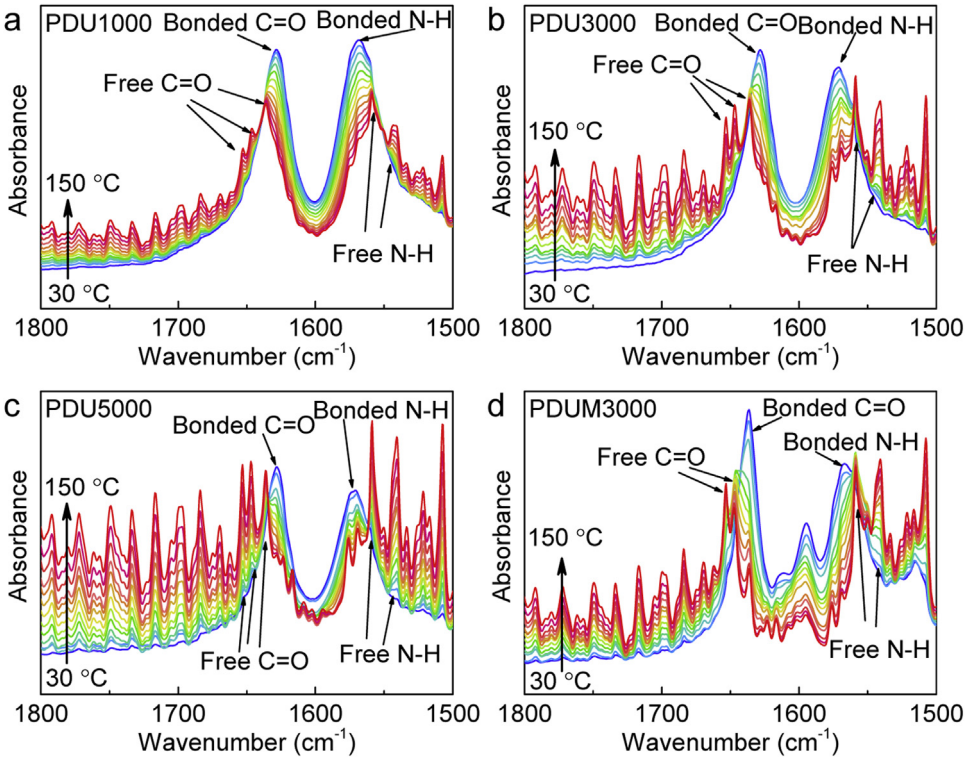

Fig. 2. *In situ* **ATR-FTIR spectra obtained from PDU1000** (a)**, PDU3000** (b)**, PDU5000** (c) **and PDUM3000** (d)**, at an increasing temperature from 30 °C to 150 °C.**

stretching region (3600~3100 cm^{-1}, Fig. S5) the broad bands at ~3330 cm^{-1} correspond to the stretching of hydrogen bonded N—H, showing a decrease with increasing temperature. Meanwhile, new peaks at higher frequency, representing the free N—H, arisen and increased. In summary, the evolution of the ATR-FTIR spectra as the temperature was increasing clearly indicates the breakage of hydrogen bonds and the generation of free C=O and N—H in all the considered samples. Notably, the changes in the signals obtained from PDU3000 and PDU5000 were more pronounced than from PDU1000 and PDUM3000, which implies relatively easier breakage of hydrogen bonds in the PDU3000 and PDU5000 samples (Fig. 2).

2.2. Self-healing and mechanical properties

The self-healing and mechanical properties of PDU and PDUM were investigated by means of the uniaxial tensile test. For this purpose, self-healed polymer samples subjected to mechanical damage by a cut with a scalpel were compared with pristine uncut samples. As shown by the stress-strain curves in Fig. 3a–d, the samples not subjected to cutting show largest extensibility (black curves). The elongation at breakage of the PDU samples increases with the molecular weight of free segment (PDMS), while a reverse trend was observed for the Young's modulus, *i.e.* decreasing from 20.71 ± 0.60 MPa to 0.28 ± 0.02 MPa (Fig. S6). Given that the PDU

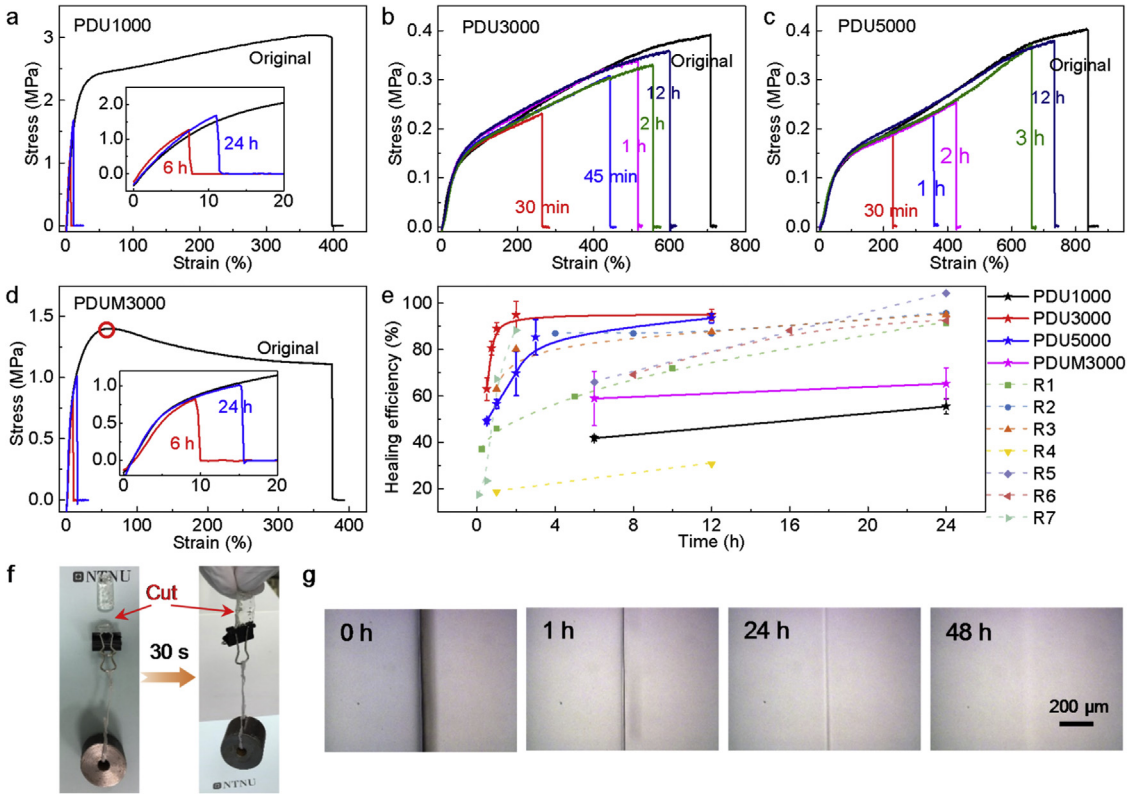

Fig. 3. Self-healing properties and mechanical properties of the elastomers at room temperature. Stress-strain curves obtained for the original and self-healed PDU1000 (a), PDU3000 (b), PDU5000 (c), and PDUM3000 (d). (e) Healing efficiency of PDU, PDUM, and other previously reported elastomers (R1 [23], R2 [24], R3 [26], R4 [35], R5 [21], R6 [36] and R7 [27]). (f) Self-healing capability of the PDU3000 sample with cross-sectional area of ~0.25 cm^2 cut in half by a scalpel (left). The lifted weight after self-healing is ~93 g (right). (g) Optical microscopy images of scratched PDU3000 during the self-healing process. All of the optical microscopy images share the same scale bar. The insets in (a) and (d) are the magnified versions.

chains are cross-linked by hydrogen bonds, the hydrogen-bonding density decreases with increasing molecular weight of the PDMS segment, which is responsible for the decrease of Young's moduli among the samples. Such results agree with predictions given by the classical polymer physics theory [39],

$$E \sim \frac{1}{N_x} \quad (1)$$

where E and N_x are the elastic modulus and the number of monomers between two crosslinking points (the length of the free segments), respectively. It should be noted that the stress-strain curve of PDUM3000 (Fig. 3d) was different from that of the PDU (Fig. a–c). Although PDUM3000 possesses the same N_x as PDU3000, its Young's modulus is much higher, as shown in Fig. S6. The stress-strain curve obtained from PDUM3000 shows a distinct necking point (ultimate tensile strength indicated by the red circle in Fig. 3d) at the early stage of the tensile test. After the necking, the stress-strain curve features a gradual decrease before failure. The difference between PDUM3000 and PDU3000 is attributed to their different molecular structures, leading to different degrees of crystallinity, which will be discussed in the following text.

To establish the self-healing potential in the materials, the samples were first cut in halves, which were then aligned and brought together in contact again for healing, during varying healing times at room temperature, before subjected to the tensile test. As shown in Fig. 3a–d, the tensile strength of all the healed samples increases universally with the healing time. Most interestingly, PDU3000 and PDU5000 exhibited a pronounced self-healing ability, showing large elongation (over 200 %) at breakage within 30 min of self-healing. In contrast, PDU1000 and PDUM3000 presented nearly no self-healing ability even when for healing times up to 24 h. In order to quantify the self-healing capacity, we used the healing efficiency, defined as the ratio of the tensile strength of the healed sample to the original non-damaged sample [21,23,24,26,27,35,36]. The healing efficiency of the samples varies with the healing time, as shown in Fig. 3e. PDU3000 and PDU5000 displayed healing efficiencies of 62.9 ± 4.9 % and 49.1 ± 0.9 %, respectively, within 30 min, extending the upper bound when considering all other self-healing polymeric materials reported in the literature. As the healing time increased to 12 h, the healing efficiency of PDU3000 and PDU5000 further increased to a stable and striking value exceeding 90 %. The trend of the healing efficiency coincides with the diffusion-reaction model proposed by Yu et al. [33]. Comparing with previous reports (Fig. 3d) [21,23,24,26,27,35,36], the two self-healing elastomers PDU3000 and PDU5000, locate in the upper left corner of Fig. 3e, indicating outstanding self-healing rates. Especially, PDU3000 shows the fastest healing rate with healing efficiencies up to more than 80 % and 90 % within healing times of 45 min and 2 h, respectively. To visualize the ultrafast self-healing ability of PDU3000, a sample was cut into two pieces, which were then aligned and brought together in contact. In a short time period of 30 s, the healed sample was able to sustain a stress of ~36.5 kPa, as shown in Fig. 3f and Movie S1. In addition, the healing process of PDU3000 and PDU5000 after a cut in the surface was monitored by optical microscopy, as shown in Figs. 3g and S7. The two halves of PDU3000 adjacent to the cut is seen to move closer apace in 1 h. Afterwards, the cut developed into a slight indentation after 24 h and almost disappeared (where no pronounced difference between the cut and intact surface is observed) with a prolonged healing time of 48 h (Fig. 3g). A similar self-healing process was also observed in PDU5000, as shown in Fig. S7.

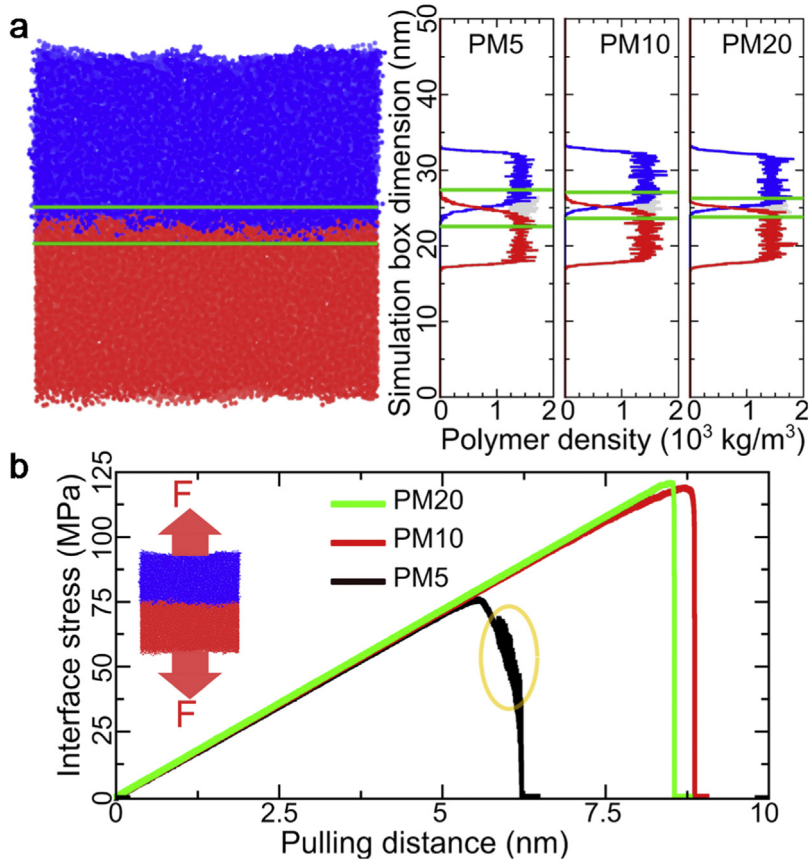

Fig. 4. Healing Interface thickness and detachment under stress. (a) Representative snapshot of the coarse-grained models of two identical polymer blocks in the three systems, PM5, PM10 and PM20, after 2 μs healing simulation (left), with the interface marked by green lines. The thickness of the interface was defined as the distance between two front density ends of the two polymer blocks, with density profiles given on the right. The density profiles of the two polymer blocks display the same color as in the snapshot. Total density profiles of the systems are shown in grey. (b) Representative interface stress profiles were monitored upon detachment of the two polymer blocks in each system. The force loading mode is shown in the inset. Stress fluctuations resulting from polymer creeping in the PM5 is highlighted by the yellow circle.

2.3. Fast self-healing mechanism

In order to understand the atomistic interactions and polymer chain dynamics at the self-healing interface, atomistic modelling and molecular dynamics (MD) simulations were carried out with coarse-grained polymer systems that qualitatively feature the experimental systems. As shown in Fig. 4 and by modelling details given the Materials and Methods Section in the Supplementary Materials, three polymer systems, termed PM5, PM10, and PM20, with varied density of strong interaction sites (representing hydrogen bonds) were built for self-healing and detachment simulations (Fig. S8). Briefly, all these three systems contained two identical blocks of 10 well-mixed 200-monomer chains. Each polymer in the PM5 system contained 5 strong interactions sites evenly distributed along the chain, while the ones in the PM10 and PM20 systems contained 10 and 20 strong interaction sites, respectively. The two blocks of polymer in each system were let to adhere (heal) for 2 μs, and then were detached from each other by pulling forces for accessing the interface robustness (Fig. S9).

The properties of the polymer healing interface were determined by the density of strong interaction sites in the polymer. The adhesion potential of the healing interface showed an inverse correlation with the strong interaction site density in the three systems. During the healing time of 2 μs, the healing interface in the PM5 system reached the lowest adhesion potential despite the lowest density of strong interaction sites among the systems, as shown in Fig. S10. Interestingly, a lower density of strong interaction sites in the system led to a higher fluctuation of the interface adhesion potential, meaning higher chain mobility at the healing interface, which further resulted in varied healing interface thickness in the three systems at the end of the healing simulations. As shown in Fig. 4a, the healing interface thickness was ~5 nm in the PM5 system, significantly higher than ~3 nm and ~2 nm in the PM10 and PM20 systems, respectively, at the end of the 2 μs healing simulations.

Adhesion strength of the healing interface in three systems was probed by counter pulling force acting on the two identical polymer blocks in each system, as depicted in Fig. 4b. The pulling force monitored in five independent simulations of each system was normalized by the cross-sectional area of the simulation system, which yielded the interface adhesion stress. Although the healing interface in the PM20 system is the thinnest (Fig. 4a), it yet showed the highest rupture stress of 122.1 ± 1.8 MPa, outperforming the healing interfaces in PM10 (119.7 ± 1.1 MPa) and PM5 (77.4 ± 1.8 MPa). The high interface rupture stress in PM20 can be attributed to the high strong interaction site density, the key role of reforming a strong interface. Interestingly, the healing interface in PM10 seemed more ductile than in the PM20, as longer pulling displacement was needed for detaching the interface, as shown by the representative stress profiles in Fig. 4b. It is worth noting that distinguishing fluctuations were observed in the stress profiles right after the peak stress value in detaching the healing interface in the PM5 system (yellow circle, Fig. 4b), which indicates different interface failure mechanisms in this system compared to PM10 and PM20. Indeed, the healing interfaces in both PM10 and PM20 detached following an adhesive failure mode, while the two poly-

mer blocks in PM5 creeped first before being torn away from each other, as shown in Fig. S11.

In summary, the results from atomistic modelling and MD simulations indicated that the density of strong interaction sites in the polymer can significantly affect the interfacial healing dynamics and re-open mechanics under loading. With high density of strong interaction sites, for instance, hydrogen-bonding sites, the polymer system will sacrifice polymer chain mobility and become more rigid, resulting in thin healed interfaces. Despite the thin healed interface, high density of strong interaction sites can yet guarantee high interface rupture stress, which favours higher self-healing strength. With low density of strong interaction sites, the polymer chains can diffuse easily, which can result in a thicker and thus weaker healed interface. Owing to weak internal interaction in the polymer body, creeping can happen earlier under stress. The creeping behaviour of the polymer can severely hinder the interface strength and lead to failure of polymer adhesion. For achieving sufficiently thick and strong healing interfaces, it is important in experiments to look for an optimal density threshold of strong interaction sites for the highest self-healing efficiency.

The results from the atomistic modelling and MD simulations shed light on polymer design for high self-healing efficiency, and thus why PDU3000 shows the fastest self-healing rate amongst the considered samples. The self-healing properties are dominated by c_H and the flexibility of moieties, and the PDU3000 coating exhibits an optimal balance between these two factors. The c_H of PDU and PDUM is proportional to the stoichiometric ratio of the molecular formula (Fig. S12) and decreases with increasing molecular weight of the PDMS segments. Since hydrogen bonds in PDU are solely formed between the urea groups, the c_H is proportional to the atomic percent (at%) of nitrogen (N). To study the at% of N, the chemical composition of the freshly cut surfaces of PDU was investigated by X-ray photoelectron spectroscopy (XPS). The sample surfaces were etched by argon for 100 s before characterization. XPS wide scan of PDU shows the peaks of oxygen (O) 1s, N 1s, carbon (C) 1s, silicon (Si) 2p (Fig. S13). The at% of N indeed shows the same trend with the calculated c_H, *i.e.* decreasing with increasing molecular weight of the PDMS segments (Fig. S13). High at% of N on the surface favours the formation of hydrogen bonds (reaction), but leads, however, to high friction between polymer chains and thus low chain mobility, as well as poor self-healing ability. Based on the XPS results, the PDU3000 sample shows the most optimal c_H, and hence leads to the fastest self-healing rate of this study. The N—H groups can exist in two states, namely either being free (N—H) or hydrogen bonded (N—H···O). On the cut surface, bonded N—H groups hinder the mobility of the polymer chains, while free ones facilitate the healing process. The N 1s orbital of bonded N—H groups lies in a lower binding energy range than in the free N—H groups [40–42], which can be distinguished by narrow-scan XPS analysis. As shown in Fig. 5a–c, after fitting two-peak components of XPS spectra in N 1s region, the corresponding N 1s involved (bonded state, green) and uninvolved (free state, blue) hydrogen bonding can be classified. As expected, the largest percentage of bonded N—H groups is observed in PDU1000, indicating that the polymer chains are strongly restricted by hydrogen bonds in the self-healing process. In comparison, smaller portions of bonded N—H groups are expectedly observed in PDU3000 and PDU5000. In order to quantify the content of bonded and free N—H on the fresh surfaces, their atomic percent, N_b% and N_f% respectively, are calculated by

$$N_b\% = \frac{A_b}{A_b + A_f} \times N\% \tag{2}$$

$$N_f\% = \frac{A_f}{A_b + A_f} \times N\% \tag{3}$$

where N%, A_b and A_f are the atomic percent of N obtained from the wide scan, and the integrating areas corresponding to the bonded and free N (green and blue regions in Fig. 5a–c), respectively. As shown in Fig. 5d, the atomic percent of bonded N—H groups decrease with increasing molecular weight of the PDMS segment, showing the same trend as for c_H. The atomic percent of free N—H groups in PDU3000 exhibits the highest value, even higher than in PDU1000. This is thus a strong evidence that the free N—H groups underlie the fastest self-healing mechanism, which consequently enables the fastest self-healing rate in PDU3000. Comparison of PDU3000 and PDUM30000 reveals yet another important factor of self-healing. Despite the fact that PDUM3000 and PDU3000 have comparable c_H values, PDUM3000 shows negligible self-healing abilities. Because PDUM3000 contains symmetric MPI units by design, crystallization is greatly promoted in the polymer body, as confirmed by differential scanning calorimetry (DSC) in Fig. 5e [27,29]. There is an exothermic peak starting from around 60 °C in the DSC curve of PDUM3000, resulting from the crystallization of the symmetric benzene rings (Fig. 5e and f). Conversely, there is no crystalline peak observed in the DSC curves of the PDU samples (Fig. 5e). It should also be noted that the necking in the stress-strain curves of PDUM3000 is also the result of the crystalline structure [43].

Since PDU3000 demonstrated the best molecular composition for self-healing amongst the considered samples, it was subjected to cyclic tensile tests for characterization of the healing mechanism and mechanical energy dissipation (Figs. 5g–i and S14). The typical loading-unloading curves within the first 10 cyclic tests on PDU3000 at a constant strain of 200 % clearly exhibit the Mullins effect (cyclic softening), owing to the cleavage of hydrogen bonds and reconstruction of polymeric networks [44]. The hysteresis energy, which is the integrated area of the loop, decreases in each test cycle, as depicted in Fig. 5g. The hysteresis ratio, *i.e.* the ratio of hysteresis energy to loading energy (integrated area under loading curve), shows a reduction from 0.72 to 0.65 at the first two cycles and then stabilizes at a value around 0.65 (Fig. 5g). This can be attributed to the rupture of weak hydrogen bonds and reorganization of polymeric chains into a favourable orientation after the first cycle [44]. Such a high hysteresis ratio during cyclic tensile tests suggests fast chain relaxation and fast dynamic dissociation-association of hydrogen bonds in the body of the polymer. To verify the effect of time on the hysteresis ratio, another cyclic test with interval waiting time of 30 min between the first two cycles was carried out. As shown in Fig. 5h, the hysteresis ratio increased significantly after the 30 min interval time. In addition, the peak stress of the second cycle after 30 min is also larger than that without interval time at the same strain (Fig. 5h), which can be attributed to sufficient relaxation of the polymer chains and most likely reformation of a higher number of hydrogen bonds. The ratio of hysteresis energy between the second cycle and the first cycle can be defined as self-healing recovery ratio [22]. As shown in Fig. 5i, the recovery ratio of the second cycle shows a significant increase from 0.40 to 0.63 after the interval time of 30 min. Such obvious improvement in recovery ratio indicates that the elastomer can serve as an ideal candidate for self-healing materials under similar or lower mechanical operational frequency, for instance in the case of icing and de-icing cycles [16].

2.4. Anti-icing properties

Since PDU3000 exhibits the best self-healing properties, its potential for anti-icing applications was further investigated. The

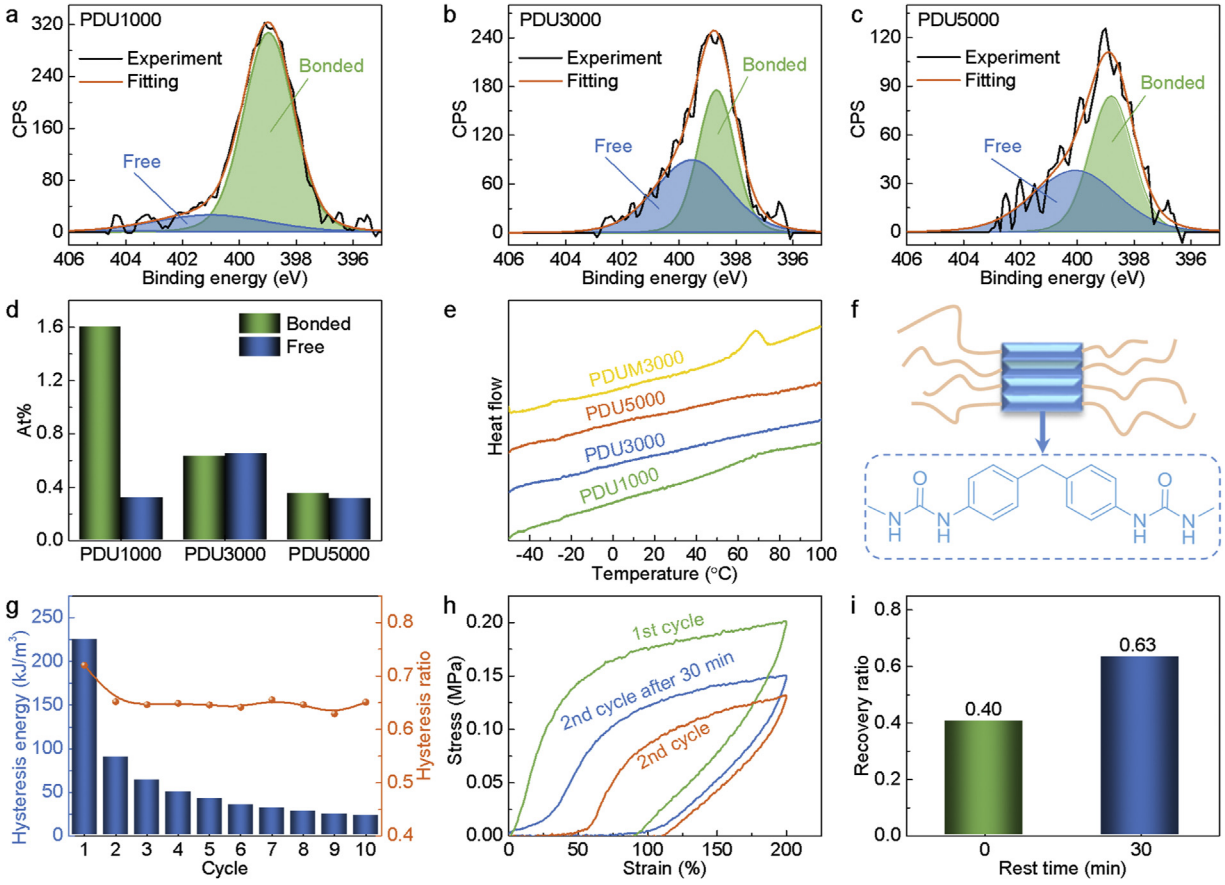

Fig. 5. Molecular structure and cyclic tensile tests of PDU. Narrow-scan XPS spectra and their fitting curves of PDU1000 (a), PDU3000 (b), and PDU5000 (c) in the N 1s region. (d) Atomic percent of hydrogen bonded and free N derived from wide and narrow scans. (e) DSC curve of the PDU samples and PDUM in the temperature range of -50 °C and 100 °C. (f) Schematic of packing and crystalline structure of PDUM3000. (g) Hysteresis energy and hysteresis ratio during the first 10 cycles of the cyclic tensile test. (h) Stress-strain curves of the 1st cycle (green), 2nd cycle (orange) and 2nd cycle after 30-min rest (blue). (i) Recovery ratio of the 2nd cycle (green) and the 2nd cycle after 30-min rest (blue).

detachment of ice from smooth coatings is an interfacial fracture process, in which the maximum ice shear strength τ is given by

$$\tau = \sqrt{\frac{EG}{\pi a \Lambda}} \tag{4}$$

where E, G, a and Λ are the elastic modulus, surface energy, crack length and a non-dimensional constant related to the geometric configuration (in some cases the geometrical contribution a can be replaced by the coating thickness t) [45,46]. In other words, elastic modulus and surface energy of the coating play important roles in terms of the ice adhesion strength. Firstly, Young's modulus of PDU3000 was found to be 0.42 ± 0.04 MPa (Fig. S6), only one-third of commercial Sylgard 184 [16]. Such low elastic modulus is in favour of the detachment of ice from the coating [12]. To study the surface energy of PDU3000, its wettability was quantified by evaluating water droplet dynamic contact angle, as shown in Fig. 6a–c. A deionized water droplet was expanded and shrunk on the sample to obtain the advancing contact angle (ACA, Fig. 6a) and receding contact angle (RCA Fig. 6b). The ACA of PDU3000 was found to be 122°, which is similar to the value of commercial Sylgard 184, confirming the hydrophobicity and low surface energy of the coating [2]. However, the PDU3000 molecule itself is amphiphilic, because it contains both hydrophobic PDMS segments and hydrophilic urea groups. Once the coating is exposed to water, the hydrophilic parts can rearrange at the polymer-water interface, driven by the hydration energy [47]. Therefore, PDU3000 presents a low RCA of 70° and a large contact angle hysteresis (CAH) of 52°. Notably, the high mobility of PDU3000 molecule will also contribute to its dynamic polymer rearrangement in contact with water.

Overall, the low Young's modulus as well as the hydrophobicity of PDU3000, make it a competent candidate for icephobic materials in combating unwanted ice accretion [16]. Nowadays, durable passive icephobic coatings have become the most desired materials to mitigate the ice problem [2]. The fast self-healing property of PDU3000 can avoid the accumulation of mechanical damage in the icephobic coating which can lead to catastrophic failure during practical applications [16]. The icephobicity of PDU3000 was evaluated by measuring the ice adhesion strength *via* the vertical shear test [16,48], as shown in Fig. 6d. The PDU3000 coating with a thickness of 378 μm exhibited a low ice adhesion strength of 38.3 ± 0.5 kPa, which is far below the threshold of icephobicity that have been defined (< 100 kPa) [2,49] and much lower than commercial silicone (Sylgard 184: 169.6 ± 3.3 kPa) of similar thickness [16]. The low ice adhesion strength of PDU3000 is ascribed to the low surface energy as well as the low Young's modulus. Low surface energy guarantees low work of adhesion between ice and the coating, and low Young's modulus facilitates the formation of voids at the polymer-ice interface under loading, both of which favour the detachment of ice from the coating, as described by Eq. (4). Most importantly, the PDU3000 icephobic coating presents remarkable mechanical durability due to its optimized self-healing properties, showing ice adhesion strength around 50 kPa during 20 icing/deicing cycles and 48.2 ± 4.6 kPa even after the cutting/healing process (Fig. 6e). The fast self-healing ability can not only heal defects at the nano- and microscale

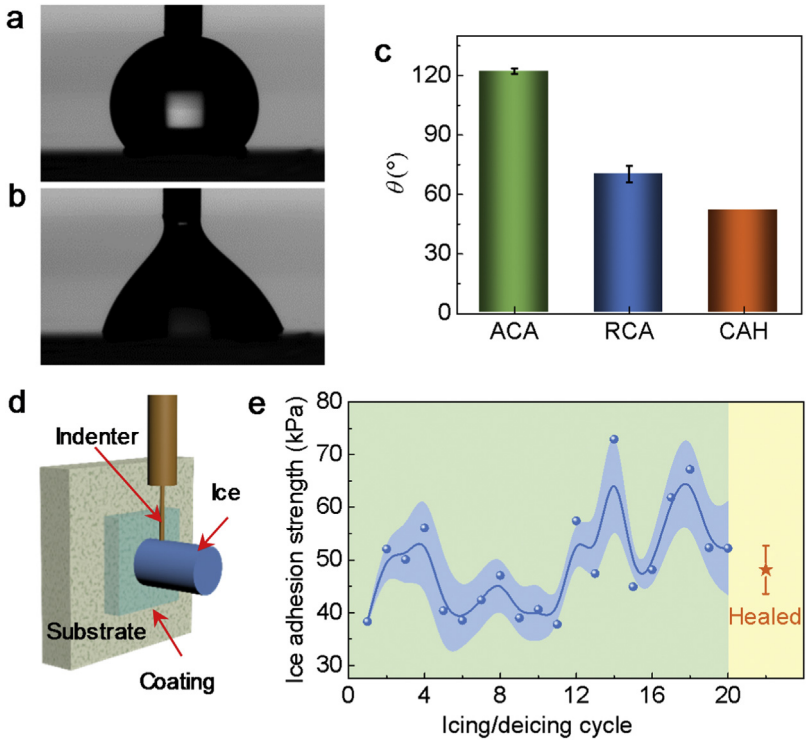

Fig. 6. Wettability and anti-icing properties of PDU3000. Image of (a) advancing contact angle and (b) receding contact angle. (c) Obtained values for the advancing contact angle (ACA), receding contact angle (RCA) and contact angle hysteresis (CAH). (d) Schematic ice adhesion test setup. (e) Ice adhesion strength of the PDU3000 coating during 20 icing/de-icing cycles (green zone), and after cut/healing test (yellow zone). The blue region during the icing/deicing cycles indicates the error.

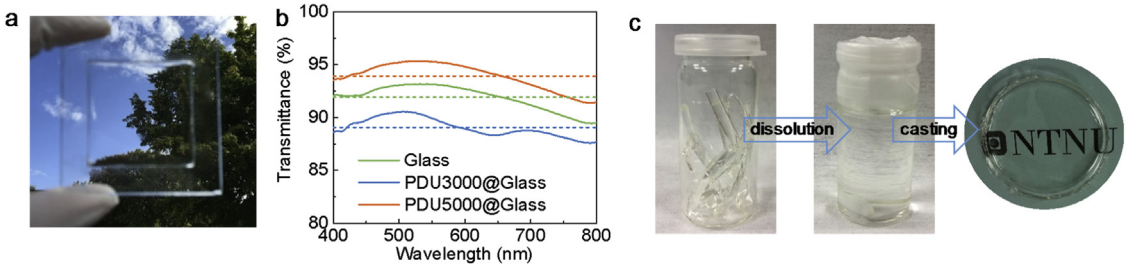

Fig. 7. Transparency and recyclability of the PDU. (a) Photograph of a glass substrate coated with PDU3000 showing the high transparency. (b) Transmittance of bare glass (green), glass coated with PDU3000 (blue), and glass coated with PDU5000 (orange). The dashed lines are the corresponding average values. (c) Broken samples were dissolved and recast to form a new transparent solid thin film.

to maintain the coating integrity during icing/deicing cycles and prevent catastrophic devastation, but can also repair mesoscale mechanical damage avoiding the ice interlocking effect.

2.5. Transparency

When ice accretes on solar panels, windows, or sensors, the transparency will decrease rapidly, resulting in the loss of their efficiency or even dysfunction. Transparent icephobic coatings can effectively address this problem since they can maintain high transparency to the underlying substrate and reduce the accretion of ice simultaneously. However, high transparency has to date not been combined with self-healing to yield both transparent and durable icephobic coatings [16,17]. As in the designed polymer, colourless segments were used in the synthesis of PDU, leading to excellent transparency with resulting phase separation detected. After applying the coating (thickness: ~350 μm) on glass, exceptionally high transparency was maintained, showing almost no visible difference with bare glass (Fig. 7a). The transmittance in visible region of bare glass, glass coated with PDU3000, and glass coated with PDU5000 were measured for detailed comparison. All the samples showed a transmittance higher than 87.5 % in the wavelength range of 400 nm–800 nm (Fig. 7b). The average transmittance of glass coated with PDU5000 reached 93.9 %, even higher than the value of bare glass (91.9 %), as shown in Fig. 7b. This effect is attributed to the lower refractive index of polymers than glasses, which means more light can pass through the surface [50]. The average transmittance of glass with coated PDU3000 also exhibited a high transmittance of 89.1 % in the visible region, only slightly lower than bare glass (Fig. 7b). The exceptionally high transmittance of the prepared coatings demonstrates that they can be applied in the situations that require high transparency to maintain their functionality.

2.6. Recyclability

Fabricating recyclable materials is a crucial way to realize a more sustainable society. However, the current state-of-the-art icephobic polymer coatings are usually covalently cross-linked networks [2,12,46,51–53], which cannot be reused. Herein, our PDU possesses good processability and is recyclable and sustainable, since

the internal dynamic hydrogen bonds easily dissociate in organic solvents, such as tetrahydrofuran, chloroform, *etc.* As shown in Fig. 7c, broken pieces of PDU3000 were dissolved in tetrahydrofuran, followed by recasting and evaporation in a petridish to obtain a solid compact thin film. The transparency of PDU is fully maintained after this recycling operation.

3. Conclusion

An icephobic coating with combined properties of ultrafast self-healing and high transparency was for the first time designed and prepared in this work. The material showed outperforming abilities to restore more than 80 % of the ultimate tensile strength after cut within 45 min of healing at room temperature. Such ultrafast self-healing rate benefits from the polymer design of flexible segments as well as the high concentration of free pairs for hydrogen bonding, with nanoscale mechanics of the healing interface elucidated by atomistic modelling and simulations. The efficient self-healing function endowed the coating with the ability to heal defects at nano- and microscale to prevent catastrophic devastation and maintain the coating integrity during icing/deicing cycles, as well as repairing the mechanical damage at the mesoscale to avoid the interlocking effect. As a result, the coating exhibited durable icephobicity, showing low ice adhesion around 50 kPa during 20 icing/deicing cycles and even after mechanical damage. Besides, the coating on a glass substrate presented a high transmittance of 89.1 %, close to the transparency of bare glass. The icephobic coating thus possesses great potential for icing protection on surfaces that require high light permeation for operation, such as solar panels, windows and sensors. The coating design in this work combines the properties of icephobicity, mechanical durability (*via* self-healing), transparency and recyclability, which shed light on materials diversity design for meeting complex environmental requirements encountered in the field of anti-icing.

Author contributions

Z. Z., J. H. and Y.Z. conceived the project. Y. Z. designed and synthesized the materials. S. X. performed the molecular dynamic simulation. Y. Z., T. L. and F. W. conducted the characterizations. Y. Z., V. H., S. X., J. H. and Z. Z. co-wrote the manuscript with the contribution and approval of all the authors. All authors discussed and commented on the manuscript.

Declaration of Competing Interest

The authors declare that they have no known competing financial interests or personal relationships that could have appeared to influence the work reported in this paper.

Acknowledgements

The Research Council of Norway is acknowledged for the support to the PETROMAKS2 Project Durable Arctic Icephobic Materials (project no. 255507) and for the support to the Norwegian Micro- and Nano-Fabrication Facility, NorFab (project no. 245963). We thank Amin Hossein Zavieh, engineer at NTNU Nanolab Norwegian University of Science and Technology, for help with XPS characterization. We also appreciate Trond Auestad at the Department of Structural Engineering at NTNU for help with mechanical testing.

Appendix A. Supplementary Materials

Materials and Methods and other supplementary figures and information are given in the online version.

Appendix B. Supplementary data

Supplementary material related to this article can be found, in the online version, at doi:https://doi.org/10.1016/j.apmt.2019.100542.

References

[1] K. Golovin, A. Dhyani, M.D. Thouless, A. Tuteja, Low-interfacial toughness materials for effective large-scale deicing, Science 364 (2019) 371–375, http://dx.doi.org/10.1126/science.aav1266.
[2] K. Golovin, S.P. Kobaku, D.H. Lee, E.T. DiLoreto, J.M. Mabry, A. Tuteja, Designing durable icephobic surfaces, Sci. Adv. 2 (2016), e1501496, http://dx.doi.org/10.1126/sciadv.1501496.
[3] M.J. Kreder, J. Alvarenga, P. Kim, J. Aizenberg, Design of anti-icing surfaces: smooth, textured or slippery? Nat. Rev. Mater. 1 (2016) 15003, http://dx.doi.org/10.1038/natrevmats.2015.3.
[4] H. Sojoudi, M. Wang, N.D. Boscher, G.H. McKinley, K.K. Gleason, Durable and scalable icephobic surfaces: similarities and distinctions from superhydrophobic surfaces, Soft Matter 12 (2016) 1938–1963, http://dx.doi.org/10.1039/c5sm02295a.
[5] L.B. Boinovich, A.M. Emelyanenko, K.A. Emelyanenko, E.B. Modin, Modus operandi of protective and anti-icing mechanisms underlying the design of longstanding outdoor icephobic coatings, ACS Nano 13 (2019) 4335–4346, http://dx.doi.org/10.1021/acsnano.8b09549.
[6] T.M. Schutzius, S. Jung, T. Maitra, P. Eberle, C. Antonini, C. Stamatopoulos, D. Poulikakos, Physics of icing and rational design of surfaces with extraordinary icephobicity, Langmuir 31 (2015) 4807–4821, http://dx.doi.org/10.1021/la502586a.
[7] P. Guo, Y. Zheng, M. Wen, C. Song, Y. Lin, L. Jiang, Icephobic/anti-icing properties of micro/nanostructured surfaces, Adv. Mater. 24 (2012) 2642–2648, http://dx.doi.org/10.1002/adma.201104412.
[8] B. Liu, K. Zhang, C. Tao, Y. Zhao, X. Li, K. Zhu, X. Yuan, Strategies for anti-icing: low surface energy or liquid-infused? RSC Adv. 6 (2016) 70251–70260, http://dx.doi.org/10.1039/c6ra11383d.
[9] E. Mitridis, T.M. Schutzius, A. Sicher, C.U. Hail, H. Eghlidi, D. Poulikakos, Metasurfaces leveraging solar energy for icephobicity, ACS Nano 12 (2018) 7009–7017, http://dx.doi.org/10.1021/acsnano.8b02719.
[10] L. Mishchenko, B. Hatton, V. Bahadur, J.A. Taylor, T. Krupenkin, J. Aizenberg, Design of ice-free nanostructured surfaces based on repulsion of impacting water droplets, ACS Nano 4 (2010) 7699–7707, http://dx.doi.org/10.1021/nn102557p.
[11] C. Urata, G.J. Dunderdale, M.W. England, A. Hozumi, Self-lubricating organogels (SLUGs) with exceptional syneresis-induced anti-sticking properties against viscous emulsions and ices, J. Mater. Chem. A 3 (2015) 12626–12630, http://dx.doi.org/10.1039/C5TA02690C.
[12] D.L. Beemer, W. Wang, A.K. Kota, Durable gels with ultra-low adhesion to ice, J. Mater. Chem. A Mater. Energy Sustain. 4 (2016) 18253–18258, http://dx.doi.org/10.1039/c6ta07262c.
[13] T.S. Wong, S.H. Kang, S.K. Tang, E.J. Smythe, B.D. Hatton, A. Grinthal, J. Aizenberg, Bioinspired self-repairing slippery surfaces with pressure-stable omniphobicity, Nature 477 (2011) 443–447, http://dx.doi.org/10.1038/nature10447.
[14] Y. Wang, X. Yao, S. Wu, Q. Li, J. Lv, J. Wang, L. Jiang, Bioinspired solid organogel materials with a regenerable sacrificial alkane surface layer, Adv Mater 29 (2017), http://dx.doi.org/10.1002/adma.201700865.
[15] J. Chen, Z. Luo, Q. Fan, J. Lv, J. Wang, Anti-ice coating inspired by ice skating, Small 10 (2014) 4693–4699, http://dx.doi.org/10.1002/smll.201401557.
[16] Y. Zhuo, V. Håkonsen, Z. He, S. Xiao, J. He, Z. Zhang, Enhancing the mechanical durability of icephobic surfaces by introducing autonomous self-healing function, ACS Appl. Mater. Interfaces 10 (2018) 11972–11978, http://dx.doi.org/10.1021/acsami.8b01866.
[17] Y. Yu, B. Jin, M.I. Jamil, D. Cheng, Q. Zhang, X. Zhan, F. Chen, Highly stable amphiphilic organogel with exceptional anti-icing performance, ACS Appl. Mater. Interfaces 11 (2019) 12838–12845, http://dx.doi.org/10.1021/acsami.8b20352.
[18] H.J. Yang, Y.T. Pei, J.C. Rao, J.T.M. De Hosson, S.B. Li, G.M. Song, High temperature healing of Ti2AlC: On the origin of inhomogeneous oxide scale, Scr. Mater. 65 (2011) 135–138, http://dx.doi.org/10.1016/j.scriptamat.2011.03.031.
[19] S.H. Cho, S.R. White, P.V. Braun, Self-healing polymer coatings, Adv. Mater. 21 (2009) 645–649, http://dx.doi.org/10.1002/adma.200802008.
[20] M. Liu, P. Liu, G. Lu, Z. Xu, X. Yao, Multiphase-assembly of siloxane oligomers with improved mechanical strength and water-enhanced healing, Angew. Chem. Int. Ed. Engl. 57 (2018) 11242–11246, http://dx.doi.org/10.1002/anie.201805206.
[21] X. Yan, Z. Liu, Q. Zhang, J. Lopez, H. Wang, H.C. Wu, S. Niu, H. Yan, S. Wang, T. Lei, J. Li, D. Qi, P. Huang, J. Huang, Y. Zhang, Y. Wang, G. Li, J.B. Tok, X. Chen, Z. Bao, Quadruple H-Bonding Cross-Linked Supramolecular Polymeric Materials as Substrates for Stretchable, Antitearing, and Self-Healable Thin Film Electrodes, J. Am. Chem. Soc. 140 (2018) 5280–5289, http://dx.doi.org/10.1021/jacs.8b01682.
[22] Y. Song, Y. Liu, T. Qi, G.L. Li, Towards dynamic but supertough healable polymers through biomimetic hierarchical hydrogen-bonding interactions,

Angew. Chemie Int. Ed. 57 (2018) 13838–13842, http://dx.doi.org/10.1002/anie.201807622.
[23] Y. Chen, A.M. Kushner, G.A. Williams, Z. Guan, Multiphase design of autonomic self-healing thermoplastic elastomers, Nat. Chem. 4 (2012) 467–472, http://dx.doi.org/10.1038/nchem.1314.
[24] C.H. Li, C. Wang, C. Keplinger, J.L. Zuo, L. Jin, Y. Sun, P. Zheng, Y. Cao, F. Lissel, C. Linder, X.Z. You, Z. Bao, A highly stretchable autonomous self-healing elastomer, Nat. Chem. 8 (2016) 618–624, http://dx.doi.org/10.1038/nchem.2492.
[25] Y. Cao, T.G. Morrissey, E. Acome, S.I. Allec, B.M. Wong, C. Keplinger, C. Wang, A transparent, self-healing, highly stretchable ionic conductor, Adv Mater 29 (2017), http://dx.doi.org/10.1002/adma.201605099.
[26] A. Rekondo, R. Martin, A. Ruiz de Luzuriaga, G. Cabañero, H.J. Grande, I. Odriozola, Catalyst-free room-temperature self-healing elastomers based on aromatic disulfide metathesis, Mater. Horiz. 1 (2014) 237–240, http://dx.doi.org/10.1039/c3mh00061c.
[27] S.M. Kim, H. Jeon, S.H. Shin, S.A. Park, J. Jegal, S.Y. Hwang, D.X. Oh, J. Park, Superior toughness and fast self-healing at room temperature engineered by transparent elastomers, Adv Mater 30 (2018), http://dx.doi.org/10.1002/adma.201705145.
[28] M.W. Urban, D. Davydovich, Y. Yang, T. Demir, Y. Zhang, L. Casabianca, Key-and-lock commodity self-healing copolymers, Science 362 (2018) 220–225, http://dx.doi.org/10.1126/science.aat2975.
[29] Y. Yanagisawa, Y. Nan, K. Okuro, T. Aida, Mechanically robust, readily repairable polymers via tailored noncovalent cross-linking, Science 359 (2018) 72–76, http://dx.doi.org/10.1126/science.aam7588.
[30] G. Gao, G. Du, Y. Sun, J. Fu, Self-healable, tough, and ultrastretchable nanocomposite hydrogels based on reversible polyacrylamide/montmorillonite adsorption, ACS Appl. Mater. Interfaces 7 (2015) 5029–5037, http://dx.doi.org/10.1021/acsami.5b00704.
[31] Y. Yang, D. Davydovich, C.C. Hornat, X. Liu, M.W. Urban, Leaf-inspired self-healing polymers, Chem (2018), http://dx.doi.org/10.1016/j.chempr.2018.06.001.
[32] Z.P. Zhang, M.Z. Rong, M.Q. Zhang, Mechanically Robust, Self-Healable, and Highly Stretchable "Living" Crosslinked Polyurethane Based on a Reversible C□C Bond, Adv. Funct. Mater. 28 (2018), 1706050, http://dx.doi.org/10.1002/adfm.201706050.
[33] K. Yu, A. Xin, Q. Wang, Mechanics of self-healing polymer networks crosslinked by dynamic bonds, J. Mech. Phys. Solids 121 (2018) 409–431, http://dx.doi.org/10.1016/j.jmps.2018.08.007.
[34] Y. Yang, M.W. Urban, Self-healing polymeric materials, Chem. Soc. Rev. 42 (2013) 7446–7467, http://dx.doi.org/10.1039/c3cs60109a.
[35] J. Wu, L.H. Cai, D.A. Weitz, Tough self-healing elastomers by molecular enforced integration of covalent and reversible networks, Adv Mater 29 (2017), http://dx.doi.org/10.1002/adma.201702616.
[36] Q. Zhang, C.Y. Shi, D.H. Qu, Y.T. Long, B.L. Feringa, H. Tian, Exploring a naturally tailored small molecule for stretchable, self-healing, and adhesive supramolecular polymers, Sci. Adv. 4 (2018) eaat8192, http://dx.doi.org/10.1126/sciadv.aat8192.
[37] J. Cao, C. Lu, J. Zhuang, M. Liu, X. Zhang, Y. Yu, Q. Tao, Multiple hydrogen bonding enables the self-healing of sensors for human-machine interactions, Angew. Chem. Int. Ed. Engl. 56 (2017) 8795–8800, http://dx.doi.org/10.1002/anie.201704217.
[38] D.J. Skrovanek, S.E. Howe, P.C. Painter, M.M. Coleman, Hydrogen-bonding in polymers - infrared temperature studies of an amorphous polyamide, Macromolecules 18 (1985) 1676–1683, http://dx.doi.org/10.1021/ma00151a006.
[39] C. Creton, 50th anniversary perspective: networks and gels: soft but dynamic and tough, Macromolecules 50 (2017) 8297–8316, http://dx.doi.org/10.1021/acs.macromol.7b01698.
[40] R. Flamia, G. Lanza, A.M. Salvi, J.E. Castle, A.M. Tamburro, Conformational study and hydrogen bonds detection on elastin-related polypeptides using X-ray photoelectron spectroscopy, Biomacromolecules 6 (2005) 1299–1309, http://dx.doi.org/10.1021/bm049290s.
[41] W.C. Wu, D.M. Wang, Y.C. Lin, C.A. Dai, K.C. Cheng, M.S. Hu, B.S. Lee, Hydrogen bonds of a novel resin cement contribute to high adhesion strength to human dentin, Dent. Mater. 32 (2016) 114–124, http://dx.doi.org/10.1016/j.dental.2015.11.002.
[42] J.B. Gilbert, M.F. Rubner, R.E. Cohen, Depth-profiling X-ray photoelectron spectroscopy (XPS) analysis of interlayer diffusion in polyelectrolyte multilayers, Proc. Natl. Acad. Sci. U. S. A. 110 (2013) 6651–6656, http://dx.doi.org/10.1073/pnas.1222325110.
[43] A.I. Leonov, A theory of necking in semi-crystalline polymers, Int. J. Solids Struct. 39 (2002) 5913–5926, http://dx.doi.org/10.1016/s0020-7683(02)00478-x.
[44] Y. Chen, Y. Li, D. Xu, W. Zhai, Fabrication of stretchable, flexible conductive thermoplastic polyurethane/graphene composites via foaming, RSC Adv. 5 (2015) 82034–82041, http://dx.doi.org/10.1039/c5ra12515d.
[45] M.K. Chaudhury, K.H. Kim, Shear-induced adhesive failure of a rigid slab in contact with a thin confined film, Eur. Phys. J. E Soft Matter 23 (2007) 175–183, http://dx.doi.org/10.1140/epje/i2007-10171-x.
[46] Y. Zhuo, T. Li, F. Wang, V. Hakonsen, S. Xiao, J. He, Z. Zhang, An ultra-durable icephobic coating by a molecular pulley, Soft Matter 15 (2019) 3607–3611, http://dx.doi.org/10.1039/c9sm00162j.
[47] M. Inutsuka, N.L. Yamada, K. Ito, H. Yokoyama, High density polymer brush spontaneously formed by the segregation of amphiphilic diblock copolymers to the Polymer/Water interface, ACS Macro Lett. 2 (2013) 265–268, http://dx.doi.org/10.1021/mz300669q.
[48] Z. He, S. Xiao, H. Gao, J. He, Z. Zhang, Multiscale crack initiator promoted super-low ice adhesion surfaces, Soft Matter 13 (2017) 6562–6568, http://dx.doi.org/10.1039/c7sm01511a.
[49] V. Hejazi, K. Sobolev, M. Nosonovsky, From superhydrophobicity to icephobicity: forces and interaction analysis, Sci. Rep. 3 (2013), http://dx.doi.org/10.1038/srep02194 http://www.nature.com/srep/2013/130712/srep02194/abs/srep02194.html#supplementary-information.
[50] T. Li, J. He, A facile hybrid approach to high-performance broadband antireflective thin films with humidity resistance as well as mechanical robustness, J. Mater. Chem. C 4 (2016) 5342–5348, http://dx.doi.org/10.1039/c6tc01540a.
[51] F. Wang, S. Xiao, Y. Zhuo, W. Ding, J. He, Z. Zhang, Liquid layer generators for excellent icephobicity at extremely low temperatures, Mater. Horiz. (2019), http://dx.doi.org/10.1039/c9mh00859d.
[52] Y. Wang, X. Yao, J. Chen, Z. He, J. Liu, Q. Li, J. Wang, L. Jiang, Organogel as durable anti-icing coatings, Sci. China Mater. 58 (2015) 559–565, http://dx.doi.org/10.1007/s40843-015-0069-7.
[53] Y. Zhuo, F. Wang, S. Xiao, J. He, Z. Zhang, One-step fabrication of bioinspired lubricant-regenerable icephobic slippery liquid-infused porous surfaces, ACS Omega 3 (2018) 10139–10144, http://dx.doi.org/10.1021/acsomega.8b01148.